

# Introduction to continuous-wave Doppler lidar

Chris Slinger<sup>1</sup>, Michael Harris,  
*ZephIR Ltd., Natural Power, The Old Barns, Fair Oaks Farm,  
Hollybush, Nr. Ledbury HR8 1EU, U.K.*

## 1. Introduction

Remote sensing offers the wind industry an attractive alternative or complement to the traditional methods for obtaining accurate wind measurements that involve the siting of tall masts. Laser anemometry (lidar) is now demonstrating its potential for resource assessment, power curve measurement, and turbine mounted deployment for advance wind speed detection. Widespread acceptance of lidar by the industry requires that this technique be extensively validated, aiming towards a certifiable and traceable measurement standard and formal accreditation of lidar methods for different applications in a range of terrain types. This chapter outlines the lidar measurement process and capabilities specifically for the case of continuous wave (CW) systems.

Wind lidar systems were first demonstrated in the 1970's [Jelalian, 1992] and have since been applied to a wide variety of applications including aviation and meteorology. Although applications to wind energy were explored in the 1980's [Hardesty and Weber, 1987; Vaughan and Forrester, 1989], the lidar systems that existed at that time were too large and expensive to achieve serious acceptance in the industry. The situation has now changed dramatically, with rapid growth of the wind industry coinciding with development of a new generation of lidars based on optical fibre and other components that emerged from the telecommunications boom of the 1990's. The first all-fibre lidars were demonstrated in the late 1990's, and a commercial prototype unit (ZephIR) was mounted on a turbine to demonstrate wind speed detection in front of the rotor plane in early 2003. A demonstration of ground-based wind profiling followed shortly afterwards. ZephIR is a CW coherent lidar system, and this approach was selected as a means to combine simplicity with high sensitivity at ranges relevant to wind energy, and hence achieve a robust, reliable system at relatively low cost. Following this pioneering work, the pace of development has accelerated, with lidar increasingly becoming an established tool in the wind industry.

Section 2 provides an overview of lidar techniques and technology. Different types of lidar system are surveyed, and the generic physical principles underlying their operation are reviewed. The specific case examined in detail here is that of wind profiling by a ground-based conically-scanned continuous-wave (CW) lidar, rapidly becoming established as a powerful tool in the wind energy industry, and exemplified by the ZephIR lidar, initially developed by QinetiQ and now Natural Power. A number of assumptions must be made in order to extract values of wind speed from raw lidar data; these are reviewed in section 3. The different steps that are required during the end-to-end measurement process in order to arrive at a value of wind speed are detailed in section 4. It is important to understand the potential sources of error and uncertainty, and these are reviewed and analysed in section 5. Section 6 examines the important requirement for lidar calibration and traceability. Finally, section 7 draws together some conclusions and a summary of the future outlook for lidar in wind energy.

---

<sup>1</sup> chrissl@naturalpower.com

## 2. Basic principles of lidar operation and system description

### 2.1 Brief survey of lidar types

There are many different types of lidar [Jelalian, 1992] and these are capable of performing a diverse range of tasks (e.g. 3D imaging and range finding, gas species detection, remote measurement of vibrations). We concern ourselves here specifically with systems for the measurement of wind speed in the atmosphere [Zak, 2003]. Such systems fall into two broad categories: coherent lidar and direct detection lidar. Coherent lidar measures Doppler shifts by comparing the frequency of backscattered radiation to that of a reference beam via a light beating process, whereas direct detection lidar [Chanin et al, 1989] performs its frequency-shift measurements by passing the light through an optical filter, such as a Fabry-Perot etalon. By operating in the ultra-violet, direct detection lidars can exploit molecular scattering processes, guaranteeing signal returns even in very clean air where there is an absence of scattering particles.

Coherent wind lidar systems can be categorised according to their emission waveform (pulsed or continuous), waveband (visible, near-IR, far-IR), and their transmit/receive geometry (monostatic or bistatic). These notes concentrate specifically on continuous-wave (CW) coherent monostatic lidar systems that operate in the telecommunications near-IR band around  $1.55\mu\text{m}$  [Karlsson et al, 2000]; at this wavelength reliable components including optical fibre are readily available. Such systems can route the light within the lidar via fibre cables (creating an “all-fibre lidar”), rather than use mirrors to direct the beams in free space. This confers an enormous design advantage, simplifying alignment and improving robustness. Pulsed all-fibre lidar has also been developed as reported in [Pearson et al (2002)] and is discussed in other chapters.

### 2.2 Principles underlying anemometry by coherent laser radar (CLR)

The principle by which coherent lidar measures the velocity of a target is simple: a beam of coherent radiation illuminates the target, and a small fraction of the light is backscattered into a receiver. Motion of the target along the beam direction leads to a change  $\delta v$  in the light's frequency via the Doppler shift: motion towards the lidar brings about a compression of the wave and an increase in its frequency (a “blue shift”), while movement away stretches the wave reducing its frequency (a red shift). This frequency shift is measured accurately by mixing the return signal with a portion of the original beam, and sensing the resulting beats at the difference frequency on a photodetector. Like the Doppler effect, the beat phenomenon is perhaps most familiar in the context of acoustics as, for example, when two closely (but not identically) tuned guitar strings are simultaneously plucked.

The essential features are readily seen in the simplified generic CLR depicted in figure 1. In order to illustrate the concept this is drawn as a bistatic system, in which the transmit and receive optics are separate and distinct. In practice a monostatic geometry is more usual, in which the transmit and receive paths share common optics.

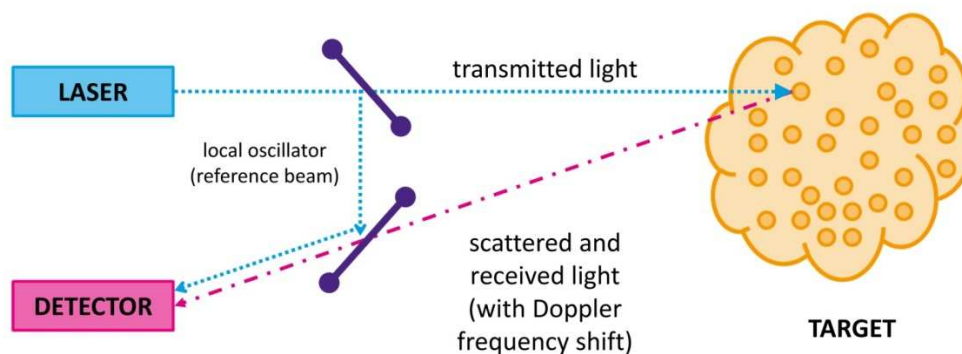


Figure 1: Generic bistatic lidar system. A small fraction of the transmitted light is tapped off by a beamsplitter to form a reference beam. This is superimposed at a second beamsplitter with the weak return scattered from moving particles. The detector picks up the resulting beat signal; this undergoes spectral analysis to determine particle velocity.

### 2.3 Role of local oscillator and range selection by focus

The reference beam, or local oscillator (LO), plays a crucial role in the operation of a CLR [Sonnenschein and Horrigan, 1971]. Firstly, it defines the region of space from which light must be scattered for detection of the beat signal; radiation from other sources (e.g. sunlight) is rejected both spatially and spectrally, so that CLR systems are usually completely immune to the effect of background light. The LO also provides a stable reference frequency to allow very precise velocity determination; as a consequence the Doppler shift measurement by a CLR system is inherently calibrated. Finally, the LO amplifies the signal via the beating process to allow operation at a sensitivity that approaches the shot-noise (or quantum) limit. This very high sensitivity permits the operation of CLR systems in an unseeded atmosphere, relying only on detection of weak backscattering from natural aerosols.

CW systems are the simplest form of lidar, possessing the advantage of reduced complexity, and their performance can be tailored closely to the wind industry's requirements. However, the overall trade-off between the pulsed and CW options for each specific application must take into account a number of factors including sensitivity, cost, velocity resolution, and maximum and minimum ranges. Unlike pulsed lidar systems, which use time of flight to discriminate between returns from different ranges, a CW lidar achieves operation at a given range by beam focusing. Wind profiling is achieved by continuously scanning the beam, focusing at a number of chosen ranges in turn. For each circular range, typically a circular scan is used. The rapid sampling rate permits 1-second "snapshots" of the flow across the scan disk at each measurement range. Focusing of the lidar beam brings about a Lorentzian spatial weighting function along the beam axis, with its peak located at the beam waist [Sonnenschein and Horrigan, 1971; Karlsson et al, 2000]. This function has a half-width given by the Rayleigh range (the distance from the waist at which the beam area has doubled).

The beam diameter at the waist increases linearly with range while the Rayleigh range increases roughly as the square. Hence the effective probe volume varies as the 4<sup>th</sup> power of the focus range, and this strong dependence has some implications for the signal statistics at shorter ranges [Harris et al, 2001b]. The minimum range for a CW lidar is very short with detection possible in principle at zero range, whereas a pulsed system is blinded while the pulse is leaving the transmitter leading to a minimum range of 10's of metres, typically around 40-50m.

### 2.4 Doppler frequency analysis and signal processing

The stages of signal processing required for CLR wind signals are discussed in Section 4.7. The detector output, containing the beat signal information embedded in broadband noise, is

typically digitised by an analogue-to-digital converter (ADC). Spectral analysis (e.g. by fast Fourier transform methods) leads to the generation of Doppler spectra. It is usually necessary to average a number of these spectra in order to improve the signal-to-noise ratio (SNR), after which the Doppler peak stands clearly above a flat shot-noise floor. A value for the line-of-sight wind speed can then be computed via a velocity estimation algorithm. This might calculate, for example, the peak or centroid value of the Doppler signal.

## 2.5 Wind profiling in conical scan mode

Since a single lidar measurement only provides the component of wind speed along the beam direction, it is necessary to scan the direction of the beam in order to generate a measurement of the wind speed vector. A conical or VAD (velocity-azimuth-display) scan pattern has been widely used [Banakh et al, 1993], see figure 2; as the beam moves, it intercepts the wind at different angles, thereby building up a series of measurements around a disk of air from which the wind speed vector can be derived. In uniform flow, a plot of the measured line-of-sight wind speed ( $V_{LOS}$ ), versus scan azimuth angle ( $\phi$ ) takes the form of a cosine wave (rectified for a homodyne lidar system that cannot distinguish the sign of the Doppler shift). The peak Doppler shifts correspond to measurements when the azimuth scan angle aligns with the upwind and downwind directions. Doppler shifts close to zero are obtained when the azimuth angle is perpendicular to the flow.

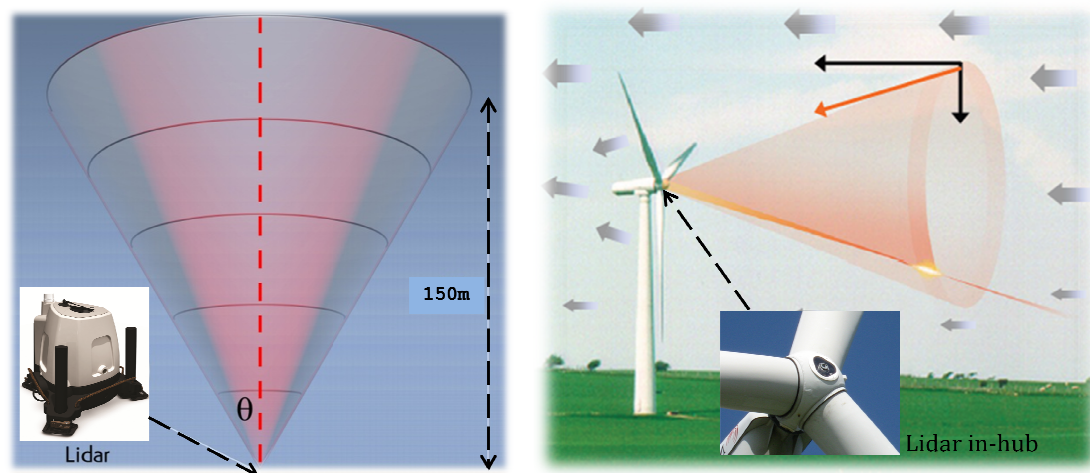


Figure 2: Conical scan pattern as used for lidar wind profiling. Left: ground based, vertical scanning. The cone half-angle ( $\theta$ ) is typically of order 30 degrees. The lidar can operate successfully even when part of its scan is obscured, e.g. by an adjacent met mast. In order to build up a wind profile, the lidar operates in a repeating sequence during which all the heights are interrogated in series. Right: one of several turbine mounted configurations, where the lidar is near horizontal and scans around a horizontal axis, usually pointing into the wind.

## 2.6 Pioneering a revolution: QinetiQ/Natural Power ZephIR lidar

Many different research groups have built and successfully deployed wind lidars over the past 30 years. However, commercial lidar products have until very recently been available from only a few companies. In 2003 the UK company QinetiQ (formerly the government-funded establishment RSRE, later DRA then DERA), launched the first commercial all-fibre lidar ("ZephIR<sup>TM</sup>") which exploits decades of research in the coherent lidar area. QinetiQ began a programme to develop a commercial fibre-based lidar in 2001; the resulting ZephIR product is now an established tool for wind profiling in the wind energy industry. Systems have been deployed successfully around the world in several demanding applications that illustrate the flexibility and robustness of the solution. Initial deployment of the ZephIR lidar (March 2003) was on the nacelle of a large (2.3MW) wind turbine (figure 3a), remotely measuring for the first time the wind speed up to 200m in front of the blades [Harris et al, 2006 and 2007]. The

lidar consisted of a 19" rack unit containing laser source, detector and signal processing computer, situated in the base of the tower, connected via over 100m of electrical and optical fibre cable to the transceiver head mounted on the top of the nacelle. The lidar system was installed and was fully operational after just a few hours, thus allowing a demonstration of advance warning of oncoming gusts and providing valuable experience in practical deployment issues.



*Figure 3: Stages of evolution of the ZephIR lidar (from top left, clockwise). The left-hand picture shows the lidar head mounted on the nacelle of a Nordex N-90 wind turbine (March 2003). The top central picture shows prototype ground-based wind profiler at Risø wind energy test site, Høvsøre, Denmark. The top right picture shows an early ZephIR production model deployed in the field. The bottom pictures show a more recent dual mode ZephIR DM300 deployed on a sea platform and also on a turbine nacelle.*

The system achieved several weeks of successful operation. It was then converted into a ground-based scanning unit for wind profiling (figure 3b). The system was first trialled in December 2003, and soon after was used in numerous campaigns in the UK, Europe, and other parts of the world. The experience gained through these trials has built confidence in the robustness and reliability of the core ZephIR technology. In late 2004, work started on a production instrument (figure 3c), designed to perform autonomous wind profiling measurements at heights up to 200m [Smith et al, 2006], primarily for site surveys at proposed wind farm sites. . The technology was transferred to Natural Power in 2007, and subsequent development resulted in the more integrated ZephIR Z300 system (figure 3d) and the dual mode DM300 which can be both turbine and ground mounted. ZephIRs have logged more than 2.8 million hours of deployment (May 2012 figures) around the world.

### 3. Lidar measurement process: Assumptions

The following sections discuss generic CW lidar considerations (most of which apply equally to pulsed systems). Where appropriate, application to the ZephIR lidar is used to provide an illustrative example.

#### 3.1 Behaviour of scattering particles

The lidar signals from which wind speeds are derived originate via backscattering of the beam by particles in the atmosphere. The constitution of these particles is generally unknown, but they are normally assumed to consist of dust, organic matter (e.g. pollen), soot, or water droplets. Knowledge of the particles' make-up is not a requirement for lidar wind speed measurement. The particles must provide sufficient signal for Doppler analysis and their motion must faithfully follow that of the wind flow. This latter assumption is very good, since viscous forces are dominant for such small particles. Larger particles for which this does not apply will rapidly fall to ground. Raindrops or snowflakes provide a strong contribution to the lidar signal. Their downward motion can lead to an error in the vertical component of wind speed (just one parameter of interest; such data can be easily identified and filtered), but the important horizontal component will be correct.

A further excellent assumption is that the return signal is dominated by light generated by single-scattering events. While it is possible for light to suffer multiple scattering in dense fog, it is a valid assumption that any effect on the Doppler spectrum is almost always negligible.

#### 3.2 Uniformity of flow and backscatter

A least-squares fitting to the variation of line-of-sight wind speed around the scan allows the derivation of wind parameters from conical scan data. These parameters pertain to a significant volume of atmosphere – the signal originates from a disk whose diameter commonly exceeds 100m, and whose depth along the beam direction can be over 10m. Except in situations of strong shear, turbulence or highly complex terrain the wind speed is reasonably uniform throughout this sampled volume, and the best fit wind parameters are used to indicate the average values over the volume. In fact, ZephIR data itself can provide a straightforward check on wind field uniformity since conical scanning provides measurements at many different scan angles; where the assumptions have broken down, measurements with less certainty can be flagged.

The contribution to the lidar signal from different regions of the lidar probe volume is weighted by the value of the atmospheric backscatter coefficient  $\beta(\pi)$  at each point. The value of  $\beta(\pi)$  is typically constant to ~10% throughout the probe volume [Banakh et al, 1993] except in conditions that lead to stable mist layers, or when the lidar beam intersects a low cloud base.

#### 3.3 Beam positional accuracy

Lidar scan angle and focus calibration are performed in the laboratory, and these must be correctly maintained throughout a period of deployment in the field. Obviously errors in the focus setting would result in wind speed measurement at the wrong height. Careful design eliminates the risk of uncertainty in the beam focus: thermal expansion, which could change the length of the transceiver telescope, can be compensated and the position of the focus mechanism can be automatically checked to provide information on any malfunction.

The lidar must be correctly set up, with the vertical and azimuthal orientation adjusted appropriately during installation. External to the lidar, it has been established that small-scale refractive-index atmospheric fluctuations will have negligible effect on the propagation of the lidar beam [Clifford and Wandzura, 1981; Lading et al, 1984].

### **3.4 Optical and electrical interference sources**

The lidar identifies the presence of a wind signal when the power density in the Doppler spectrum exceeds a threshold level. In the absence of any significant source of spurious signal, the only mechanism that can lead to such detection events is the backscatter of Doppler-shifted light into the lidar receiver. Optical interference is highly unlikely – even when the lidar points directly at the sun the spectral power density is insufficient to cause a problem, and interaction between two lidars placed side-by-side can be neglected including the possibility of interference from the beam emitted by an adjacent lidar. Careful screening eliminates the risk of spurious spectral features caused by electrical interference for any normal deployment.

### **3.5 Time-of-flight considerations**

The round-trip time for light interrogating the atmosphere at a height of 100m is less than 1 $\mu$ s. On this timescale the ZephIR scanner moves the focused beam a distance of only 300 $\mu$ m, and the laser phase drifts by an insignificant amount. The polarisation state of the lidar output is similarly frozen on this timescale.

## 4. End-to-end measurement process for CW Doppler lidar

### 4.1 Introduction

The measurement process can be split into a number of steps. This section describes these steps in turn, arriving at an overall end-to-end description of the wind speed measurement process for a CW coherent Doppler lidar wind profiler. Again, where appropriate, the ZephIR lidar is used as an example.

### 4.2 Transmitter optics

The role of the transmitter is to provide a focused beam at a desired location. This location can be moved around in space with a combination of (i) changing the focus range and (ii) passing the beam through a scanning element such as a rotating prism (wedge). Wind profiling lidars conveniently employ a conical scan with its axis aligned vertically; the cone half-angle  $\theta$  is commonly of order  $30^\circ$  (i.e. the beam elevation angle is  $\sim 60^\circ$ ). Some turbine mounted lidars use shallower scan angles, the optimum choice depending upon a variety of factor including mounting position on the turbine.

In a monostatic CW system, a Doppler-shifted contribution to the signal is generated via light scattering from any moving part of the atmosphere that the beam illuminates. The contribution from any point is weighted by the square of the beam's intensity at that point [Harris et al, 2001a]. Hence it can be shown that focusing of an ideal Gaussian beam [see, e.g., Chapters 16 and 17 of Siegman, 1986] gives rise to a spatial sensitivity along the beam direction that depends on the inverse of beam area; it follows that the sensitivity rises to a peak at the beam waist, and falls symmetrically on either side. There is also a spatial dependence of sensitivity transverse to the beam, but because the beam is very narrow this is of little interest and can be ignored. To a good approximation the axial weighting function for a continuous-wave (CW) monostatic coherent lidar is given by a Lorentzian function [Sonnenschein and Horigan, 1971; Karlsson et al, 2000]:

$$F = \frac{\Gamma/\pi}{\Delta^2 + \Gamma^2}, \quad (4.1)$$

where  $\Delta$  is the distance from the focus position along the beam direction, and  $\Gamma$  is the half-width of the weighting function to the -3dB point, i.e. 50% of peak sensitivity. Note that  $F$  has been normalised such that its integral from  $-\infty$  to  $\infty$  gives unity. To another good approximation,  $\Gamma$  is given by:

$$\Gamma = \frac{\lambda R^2}{\pi A^2}, \quad (4.2)$$

where  $\lambda$  is the laser wavelength, here assumed to be the telecommunications wavelength  $\lambda \sim 1.55 \times 10^{-6}$  m,  $R$  is the distance of the beam focus from the lidar output lens, and  $A$  is the beam radius at the output lens. The beam intensity profile is assumed to be an axially-symmetric 2D Gaussian;  $A$  is calculated for the point at which the intensity has dropped to  $1/e^2$  of its value at the beam centre. For example, if  $A$  takes the value 28mm (broadly equivalent to the current production ZephIR) then, at a focus range  $R$  of 100m,  $\Gamma$  has a value of  $\sim 5.5$ m, or a probe length (to -3dB points) of  $\sim 11$ m.

Figure 4 shows the behaviour of the theoretical sensitivity curves for the two example cases ( $A=20$ mm and 28mm) at several focus ranges. In addition the theoretical curve corresponding to one of the calibration ranges has been plotted, with experimental calibration data for comparison. Section 6 contains more detail of the calibration processes. The minimum range is determined by the focusing capability of the transceiver optics, and for ZephIR it takes the value 10m.

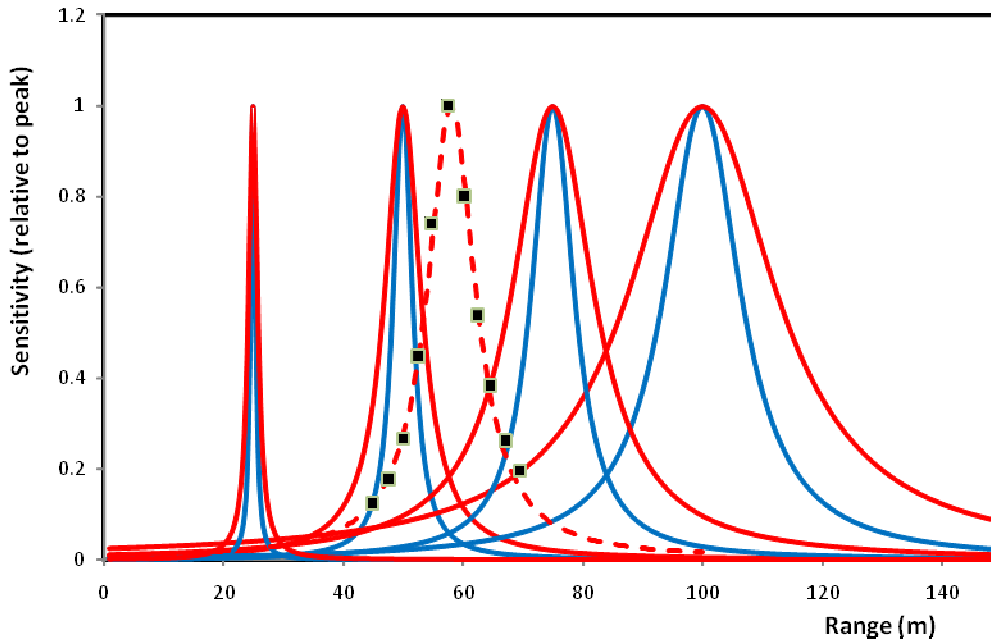


Figure 4: Theoretical lidar sensitivity curves at focus heights 25m, 50m, 75m and 100m for the two cases listed above with  $A = 20\text{mm}$  and  $28\text{mm}$ , corresponding to respectively the original (red curve) and current (blue curve) ZephIR design. The peak is normalised to unity in each case; the absolute peak value decreases as the inverse of height squared, so that the area under each curve (representing the overall sensitivity) is always the same. This illustrates a useful feature of focused CW coherent lidar that in uniform scattering, the signal-to-noise ratio is independent of focus range. Data obtained in calibration measurements (black squares) at a calibration range  $R=68\text{m}$  are in close agreement with the corresponding theoretical values (dashed curve) at the equivalent height  $58\text{m}$  ( $=68\text{m} \times \cos.30^\circ$ ). The current ZephIR design has a tighter focus than the original.

### 4.3 Light scattering by aerosols

Coherent lidar measures the Doppler shift resulting from the component of target velocity along the beam (or line-of-sight) direction. Motion of the target transverse to the beam direction produces no net Doppler shift. Hence, for a lidar at  $(0,0,0)$  measuring at a specific location  $(x,y,z)$  where wind components are  $(u,v,w)$ , the lidar will detect a line-of-sight velocity given by the dot product of the wind vector  $(u,v,w)$  and the unit vector along the beam direction:

$$V_{LOS} = \left| (u,v,w) \cdot \left( \frac{(x,y,z)}{\sqrt{x^2 + y^2 + z^2}} \right) \right| \quad (4.3)$$

Where  $V_{LOS}$  is the component of target speed along the line of sight (i.e. the beam direction), and the modulus applies to systems that cannot distinguish the sign of the Doppler shift.

In the backscattering geometry considered here, the scattered light experiences a Doppler shift in frequency given by:

$$\delta\nu = \frac{2V_{LOS}}{c} \nu = \frac{2V_{LOS}}{\lambda} \quad (4.4)$$

where  $c$  is the speed of light ( $2.998 \times 10^8 \text{ m s}^{-1}$ ), and  $\nu$  and  $\lambda$  are respectively the laser frequency and wavelength.

Since the signal originates from a finite probe length, the overall return exhibits a spectrum of frequencies. This results from the contributions from different velocities (with strengths determined by the weighting function, eqn. 4.1) over all the space occupied by the lidar beam. Note that in the absence of additional information it is not possible to identify from what position within the probe volume each component of the spectrum has originated. Section 5.2 will outline how information from additional focus ranges can be used to identify and reject spectral components originating from strongly-scattering objects (e.g. clouds) situated well outside the probe length.

For a CW coherent system, the time-averaged optical signal power  $P_S$  backscattered by the aerosols into the receiver is given to a good approximation by:

$$P_S = \pi P_T \beta(\pi) \lambda, \quad (4.5)$$

where  $P_T$  is the transmitted laser power and  $\beta(\pi)$  is the atmospheric backscatter coefficient in  $(\text{m sr})^{-1}$ . It is notable that eqn. (4.5) contains no dependence on either the focus range or the system aperture size. With a value of  $10^{-8} (\text{m sr})^{-1}$  for  $\beta(\pi)$  in clear boundary-layer air, a transmitted power  $P_T \sim 1 \text{ W}$  and  $\lambda \sim 1.5 \mu\text{m}$ , the received power  $P_S$  derived from (4.5) is only of order  $5 \times 10^{-14} \text{ W}$  emphasising the need for high sensitivity.

#### 4.4 Receiver optics

In a monostatic system, the backscattered light returns through the transmission optics (the word *transceiver* is commonly used to denote this dual role). Any motion of the beam due to scanning over the timescale for the radiation to travel to the aerosols and back will result in misalignment of the receiver, but this is insignificant for the range of parameters considered here.

After entering the transceiver, optical means are used to isolate the return light, and this is passed to the next stages of the detection process.

#### 4.5 Light beating

In coherent laser radar, the incoming Doppler-shifted radiation is optically mixed with a reference or local oscillator (LO) beam. The mixing of two waves in this manner leads to the well-known “beat” phenomenon in which the resulting amplitude oscillates at the difference frequency. In lidar, the process conveniently “downmixes” the optical frequency of the Doppler shifted return at  $\sim 2 \times 10^{14} \text{ Hz}$  to a more manageable signal in the MHz range. The efficiency of the beating process is optimised when the signal and LO beams overlap perfectly in space (i.e. they occupy identical spatial “modes”). This condition is ensured when both beams propagate in the same single-mode optical fibre, assuming that they share the same polarisation state.

It is instructive to consider a simple classical description of the light beating process. Superposition of a LO field  $E_{LO} \cos \omega_{LO} t$  and a stable signal field  $E_S \cos \omega_S t$  results in a fluctuating detector output:

$$i(t) \propto [E_{LO} \cos \omega_{LO} t + E_S \cos \omega_S t]^2 \quad (4.6)$$

This is conveniently separated into a “constant” term and a cross term oscillating at the difference frequency:

$$i(t) \propto [E_{LO}^2 + E_S^2] + 2E_{LO} E_S \cos[(\omega_S - \omega_{LO})t]. \quad (4.7)$$

Since the optical power of the local oscillator beam typically exceeds that of the signal beam by many orders of magnitude, the first term is given by  $E_{LO}^2$  to a very good approximation, quantum fluctuations on which give rise to the shot noise floor of the instrument (section 4.6). For a system for which there is no frequency shift between the LO and transmitted beams, the measured Doppler shift is given simply by:

$$\delta\nu = 2\pi |(\omega_S - \omega_{LO})| \quad (4.8)$$

from which the value of  $V_{LOS}$  is derived via (4.4). In practice a signal field originating from atmospheric scattering exhibits fluctuations in both its amplitude and phase (or frequency). The coherent detection process ensures that these properties are reproduced in the detector output so that, in the limit of high SNR, its spectral analysis gives a correct representation of the scattered light's spectrum [Harris et al, 1994].

The coherent detection process described above is also commonly referred to as homodyne or heterodyne detection. A rigorous quantum-mechanical theoretical treatment of the detection process is given in (Loudon, 2000). Note that although the detection process is described as coherent, the backscattered radiation itself is incoherent in nature, meaning that its phase is uncorrelated with that of either the transmitted beam or the local oscillator. The phase and intensity are typically subject to random fluctuations on a timescale that is related to the inverse of the signal bandwidth (see section 4.7).

#### 4.6 Photodetection

The beat signal is detected by directing the optically-mixed beam onto a photodetector which measures fluctuations in the light's intensity. In the telecommunications wavelength band around  $1.55\mu\text{m}$ , reliable photodiodes are readily available that are well suited to this purpose. The photodiode converts the incident photons into photoelectrons, which generate a measurable current (or voltage) that is normally passed through further stages of amplification before digitisation. There are generally four contributions to the output of the photodetector module:

- Dark noise – this is the intrinsic wideband noise floor generated by the detector and amplifier combination in the absence of any incident light. Dark noise is due to the random generation of electrons and holes within the depletion region of the photodetector device that are then swept by the photodetector's electric field.
- Photon shot noise [Bleaney and Bleaney, 1976] (sometimes called quantum noise) – the random generation of photoelectrons by the incident LO beam leads to a wideband, spectrally flat (white) Gaussian noise source. The shot noise power spectral density increases in proportion to the optical power of the LO beam.
- Laser relative intensity noise (RIN) – intensity fluctuations that are in excess of shot noise, caused for example by relaxation oscillation [for example, see section 25.1 of Siegman, 1986] of the laser output. For a RIN-dominated noise floor, the power spectral density increases as the square of LO power. Such oscillation is typically at relatively low frequency, peaking below 1MHz, and hence only affects the sensitivity of the lidar at low line-of-sight wind speeds around  $1\text{m s}^{-1}$ . In some systems it is possible to cancel the RIN by use of a dual-channel balanced detector.
- Beat term resulting from the wind signal – this is the contribution that contains the information on Doppler shifts from which the wind speed is derived. Its power spectral density increases in proportion both to the LO power and the signal power.

The requirements for the detector are high quantum efficiency, sufficient bandwidth to cope with the maximum Doppler frequencies of interest, and for the shot noise contribution to significantly exceed that of dark noise. This latter requirement depends on a combination of the detector's intrinsic noise floor and the optical saturation threshold.

#### 4.7 Fourier analysis and lidar sensitivity

In order to extract the Doppler frequency information, it is necessary to perform a spectral analysis of the detector output. This is conveniently done digitally; an example of a typical signal processing procedure is described below and illustrated in figure 5. An ADC with a sampling rate of 100MHz permits spectral analysis up to a maximum frequency of 50MHz, corresponding to a wind speed  $V_{LOS}$  of  $\sim 38.8\text{ m s}^{-1}$  (eqn. 4.5, with  $\lambda = 1.55\mu\text{m}$ ). A hardware low-pass filter with a cut-off frequency of 50MHz, inserted between the detector and ADC, eliminates aliasing problems. Spectra are calculated by digital Fourier transform (DFT)

methods; a 512 point DFT gives rise to 256 points in the output spectrum with a bin width of  $\sim 200\text{kHz}$ , corresponding to a line-of-sight velocity range of  $\sim 0.15\text{ m s}^{-1}$ . Each DFT represents  $\sim 5\mu\text{s}$  of data; successive DFTs are then calculated, and the resulting “voltage” spectra are squared in order to generate a power spectrum. These power spectra are then averaged to find a mean spectrum for the averaging period. The random fluctuation in the shot noise floor of the spectrum reduces as the square root of the number of averages: so the sensitivity increases by this same factor. For 4,000 averages, the measurement time amounts to  $\sim 20\text{ms}$  (or a data rate of  $\sim 50\text{Hz}$ ). This requires that the processing is capable of 100% duty cycle, which is achieved in ZephIR with a fast Fourier transform (FFT) block within a field-programmable gate array (FPGA). It has been shown that a standard fast PC with no additional duties to perform can achieve a similar performance. It is possible to accommodate reasonable variations in any of the above parameters (sample rate, DFT size, number of averages) and maintain the 100% duty cycle.

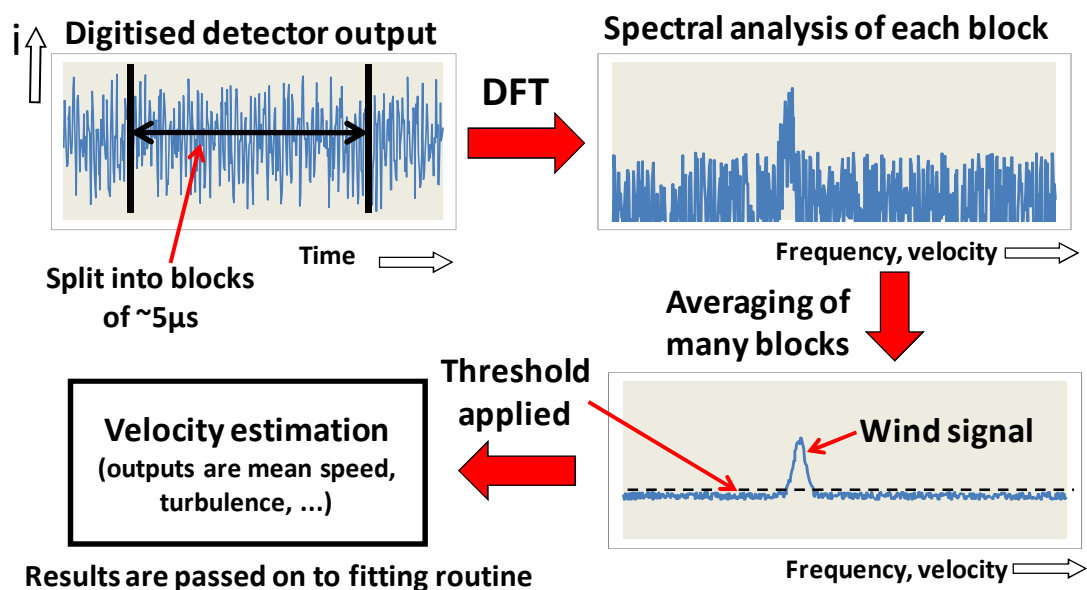


Figure 5: Stages in typical lidar signal processing: the digital Fourier transform (DFT) analysis is carried out by a computer integrated into the lidar system. As an example, 4000 individual spectra might be averaged to achieve high sensitivity and measurable returns even in very clear air. This entire process takes only 20 milliseconds, giving  $\sim 50$  measurements per second of line-of-sight wind velocity.

The width of the Doppler spectrum is determined by three elements:

- Instrumental width: this corresponds closely to the  $\sim 200\text{kHz}$  bin width mentioned above.
- Transit-time broadening: during the conical scan, the beam passes through the aerosol particles in a timescale of  $\sim 10\text{-}15\mu\text{s}$ , independent of the lidar focus setting. The corresponding broadening is again of order  $200\text{ kHz}$ .
- Turbulence broadening: the probing of a significant volume results in a range of Doppler shifts from parts of the atmosphere that are moving at different speeds (see section 4.3). In general, this contribution increases with turbulence and shear, and occasionally there is more than one peak in the spectrum as a result. There is potential scope for using this broadening to measure and characterise turbulence at a fundamental level.

The last of these usually dominates except under conditions of very uniform airflow.

High system sensitivity is of crucial importance for a wind lidar reliant on weak backscatter from the atmosphere. The signal-to-noise ratio (SNR<sup>2</sup>) for a wind speed measurement by a CW CLR is given by:

$$SNR = \frac{\eta P_s}{(hc/\lambda)\Delta\nu[1 + D(\nu) + R(\nu)]} \quad (4.9)$$

Here  $\eta$  is an efficiency term incorporating optical losses and photodetector sensitivity (typically  $\eta \sim 0.5$ , approaching the value 1.0 only for a “perfect” system),  $P_s$  is the input signal power, as defined in eqn 4.5 and  $(hc/\lambda)$  is the light quantum energy, of order  $1.3 \times 10^{-19}$  J. The signal bandwidth  $\Delta\nu$  is determined by the three contributions listed above, and the term inside the square brackets denotes the various noise sources listed in section 4.6.  $D(\nu)$  and  $R(\nu)$  represent the power spectral density (at frequency  $\nu$ ) from dark noise and RIN respectively in units of the power spectral density of the local oscillator shot noise. Ideally  $D(\nu)$  and  $R(\nu)$  should both be  $\ll 1$  over the range of Doppler frequencies of principal interest, so that the shot noise is the dominant noise source.

The SNR as defined here is the power spectral density at the Doppler peak divided by that in the surrounding noise floor. The averaging of many spectra (described in the following sections) ensures that good performance can be obtained even when the SNR is well below unity. For example, an SNR of 0.1 will easily exceed a  $5\sigma$  threshold level (see next section) for an average of 4000 spectra. From the above it is possible to derive an approximate value of  $\beta(\pi)_{min} \sim 10^{-9}$  (m sr)<sup>-1</sup> for the minimum detectable backscatter, assuming a transmitted intensity 1W and a 20ms measurement time.

#### 4.8 Velocity estimation

From the preceding sections it is apparent that each measurement of line-of-sight wind speed, obtained over a timescale of  $\sim 20$ ms, generates a Doppler spectrum consisting of one or more peaks of variable width, superimposed on a noise floor that is predominantly white, but which may have spectral features originating from RIN and dark noise sources. This section outlines steps that can be followed to derive an appropriate estimate of the wind speed.

First, the noise floor is “whitened” so that each spectral bin contains the same mean noise level, achieved by dividing the power value in each bin of the spectrum by a previously-measured value for the same bin obtained with the shutter closed. A flat threshold is then applied at a pre-determined level above the mean noise; see figure 5. A suitable and conservative choice for the threshold is 5 standard deviations ( $5\sigma$ ) above the mean noise level. In the absence of any wind signal (e.g. with the output of the lidar blocked) such a setting will give rise to negligible occurrences in which the noise alone exceeds threshold. It follows that any bin whose level exceeds the threshold is deemed to contain a valid contribution to the wind signal. For each 20ms measurement, the wind spectrum is reconstructed by subtracting the mean noise contribution from the contents of each bin that exceeds threshold, and applying a small recorection for any distortion resulting from the noise whitening. In order to proceed to the next stage, a single velocity value is derived from the resulting spectrum. A number of options are available, including peak and median values; a common solution is to calculate the mean (or centroid) value  $\langle V_{LOS} \rangle$ .

A series of these values of mean line-of-sight wind speed is generated as the ZephIR lidar performs a conical scan. Wind parameters are usually calculated from data obtained from a single revolution of the scanner. With a rotation time of  $\sim 1$  second, 50 line-of-sight values are available for the next stage, in which a least-squares fitting algorithm is applied. Data can also be generated for a 1-second, single scan rotation (based on a 50-point fit), as required by the

---

<sup>2</sup> In the lidar community, this is commonly, and more properly, referred to as the carrier-to-noise ratio (CNR)

user, and this might be more appropriate for some applications e.g. e.g. turbine control for gust detection or mechanical load mitigation.

#### 4.9 Ground based, vertical scan configurations wind field parameter determination

##### 4.9.1 Least-squares fitting routine

The data that are fed to the fitting routine consist of up to 150 pairs of values of  $\langle V_{LOS} \rangle$  and azimuth angle  $\phi$ . In conditions of uniform wind flow, this gives rise to a rectified cosine wave of the form:

$$\langle V_{LOS} \rangle = |a \cos(\phi - b) + c|. \quad (4.10)$$

The derivation of this function is straightforward and can be found in a number of publications, [e.g. Banakh et al 1993]. The peaks of the function correspond to the azimuth angle aligned parallel or anti-parallel to the wind direction. The function passes through zero when the azimuth angle is perpendicular to wind bearing since there is no component of velocity along the line of sight. The data are also conveniently displayed on a polar plot (figure 6), which provides information at a glance on the speed, direction and vertical wind component. A standard least-squares fitting routine provides the best estimates of the values of the three floating parameters (a, b and c).

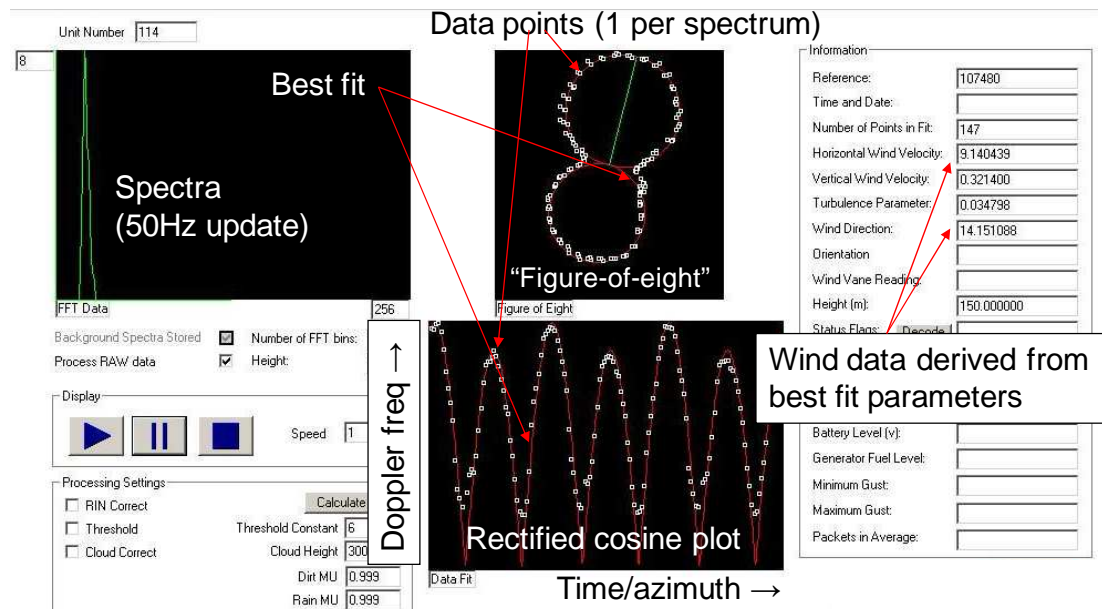


Figure 6: Wind lidar output screen, for a ground-based, vertical scan ZephIR, illustrating many of the features of a wind profile measurement. This example has been obtained at a height 150m above ground level, one of several heights being probed in sequence. The lower trace shows 147 individual line-of-sight wind speed values, obtained over a total period of 3 seconds, plotted as white squares against azimuth scan angle. The same data, along with the least-squares fit in red, are displayed above this in polar coordinates on the figure-of-eight plot showing the wind bearing to lie slightly to the E of N. The wind parameters, derived from the fit, appear in the table on the right; the horizontal wind speed at this height is determined to be 9.1 metres per second, or roughly 18 knots. The plot on the left shows just one of the spectra from which each point on the other 2 graphs is derived.

The high level of redundancy in the fitting process is advantageous and can be used to identify non-uniform flow. The root mean square deviation of the points from the optimum solution gives an indication of the quality of fit, and this can be related to the value of turbulent kinetic energy (TKE)[ see Wagner et al, 2009]. More work is needed to establish a full understanding of the turbulence information available from lidar signals [Banakh et al,

1999]. Note that information on turbulence is also available from the spectral widths of the individual line-of-sight wind speed measurements, but this is not currently used to evaluate turbulence parameters. Spectral information is commonly discarded after the velocity estimation process to minimise data volume.

#### 4.9.2 Parameter extraction

The wind parameters for each measurement period are extracted from the best fit as follows ( $\theta$  is the cone half angle of order  $30^\circ$ ):

$$\begin{aligned} \text{Horizontal speed (u)} \quad V_H &= a/\sin\theta; \\ \text{Vertical speed (w)} \quad V_V &= -c/\cos\theta; \\ \text{Bearing } B &= b, \text{ or } b \pm 180^\circ \end{aligned} \tag{4.11}$$

Where there is an ambiguity in the sign of the Doppler shift, there are two equally valid best-fit solutions corresponding to values of  $b$  separated by  $180^\circ$ . The correct choice is usually easily made by choosing the solution that lies closest to a conventional measurement from a met station situated close to ground. Conventionally, a wind profiling lidar incorporates such a station that performs these (and other) measurements and feeds the results to the analysis software.

The 1-second wind parameter values are stored internally for subsequent analysis; they can also undergo further processing for extraction of average values.

#### 4.9.3 Data averaging

It is a common requirement to calculate 10-minute averaged wind data for compatibility with industry standards. This is most easily achieved by calculation of the arithmetic mean (“scalar average”) of the individual values of  $V_H$ ,  $V_V$  and  $B$  that have been obtained during the required period. A vector average is also possible in which the resultant of the individual measurements is calculated over each 10-minute period. In practice the results from the two methods differ negligibly in reasonably stable conditions. In accordance with industry standards, ZephIR computes a scalar average for  $V_H$  and  $V_V$ , and a vector average for  $B$ .

When a CW lidar is operating as a wind profiler it is necessary to measure each height in series. Hence, at any given height the wind is not monitored continuously. Instead, an individual measurement (taking 1 to 3 seconds to obtain) is followed by a period of order 7-20 seconds during which the lidar is focused at other heights. Since this sampling is carried out randomly with respect to any behaviour of the wind, this duty cycle of order 15% has negligible impact on the validity of the resulting 10-minute averaged values. Also the typically large scan area ensures the beam samples a much higher fraction of the overall turbulent fluctuations.

#### 4.10 Least-squares fitting routine for horizontal scanning (turbine mounted) operation

The use of a CW lidar for turbine mounted applications is fundamentally a quite different arrangement when compared to a ground based, vertical scanning configuration. Unlike the latter, the scan axis is approximately horizontal, and the lidar is almost always predominantly staring into the wind. A consequence of this is that the polar plot (of the measured line-of-sight wind speeds as a function of angle) is no longer a figure of 8 shape, but instead takes on a more circular appearance. Figure 7.

Important quantities of interest for turbine relevant wind field determination include hub height horizontal wind speeds, the vertical wind shear, and the yaw misalignment. The latter is an angular measurement of the horizontal difference between the direction of the lidar scan axis and the wind direction, and it is useful for yaw control of the turbine. Horizontal shear and wind inflow angles are also of interest.

As before, a wind model can be constructed. This must take into account the mounting geometry on the turbine [e.g. Mikkelsen et al, 2010; Angelou et al, 2010]. A least squares fit of the measured wind field can be performed to extract the parameters of interest.

One of the attractive features of the CW lidar's circular scan pattern is that it samples the wind field around the full range of rotation of the turbines rotor. Typically 50 line-of-sight measurements are obtained over one circular scan in 1 second (i.e. 20 ms sample rate). This dense sampling of the wind field around the rotor disk can give valuable preview data to allow feedforward control for both collective and individual pitch control of the blades of the turbine.

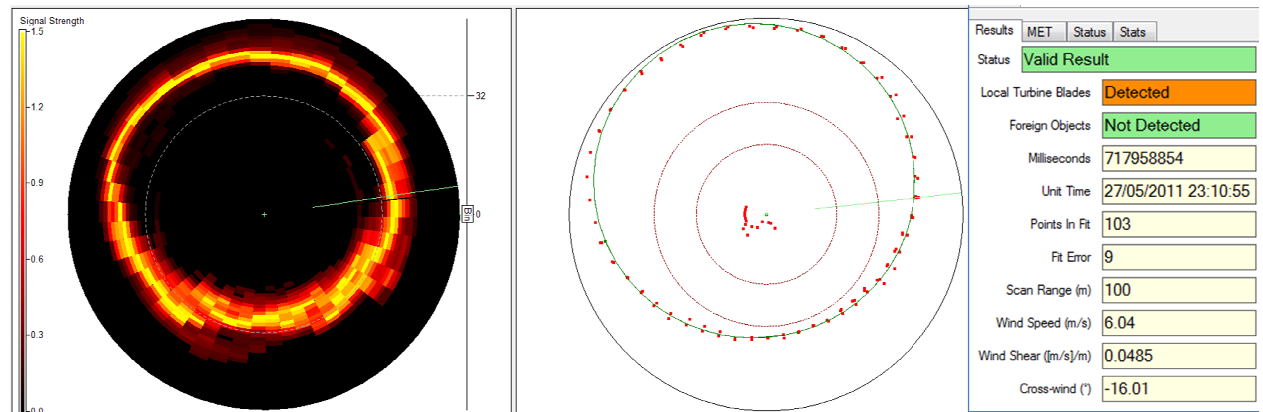


Figure 7. An example of visualisation and analysis of data from a turbine mounted ZephIR. Left: polar plot of raw data, showing line of sight wind speeds with scan angle. Radial axis is the LOS speed. The breadth and structure of plotted distribution gives an indication of the spatial turbulence within the scan volume e.g. ground induced turbulence can be seen in the lower range of angles. Low level wind jets and wakes from other turbines can also be detected in this manner. Centre: real time analysis of the received polar plot, showing centroids of the received line-of-sight speeds (red dots) and fitted wind parameters (indicated by the green closed curve). The central red dots are turbine blade returns and are filtered out automatically prior to fitting. Right: reference data and calculated wind characteristics from the green fit.

## 5. Uncertainty analysis

### 5.1 Rain/snow/cloud, solid objects

In general the Doppler shift measured by coherent laser radar is very accurate. This is apparent from eqn. 4.5 as long as the laser wavelength remains stable and the signal processing has been correctly performed – both good assumptions in practice: the laser wavelength ( $\lambda$ ) is defined by the manufacturer’s specification to within  $\pm 1\text{nm}$  of the nominal wavelength (1565nm). So the contribution to velocity uncertainty from wavelength variation is  $1/1565 = \pm 0.07\%$ . The Doppler frequency ( $\delta v$ ) spectra are calculated in a dedicated DSP board with a manufacturer’s specification of clock stability to within  $\pm 50\text{ppm}$ . The clock stability is directly proportional to uncertainty in wind velocity and therefore the uncertainty due to this potential source of error is again small at  $\pm 0.05\%$ . Finally the values of  $\langle V_{\text{LOS}} \rangle$  that are derived from the centroids of the spectra can be measured to considerably better than a bin width.

Confirming the above instrumental considerations, the line-of-sight velocity calibration was experimentally verified [Pedersen] in a recent wind-tunnel trial. A ZephIR300 configured to stare directly along the flow reported measurements in very good agreement with a reference pitot tube, for a wide range of wind speeds from 5 – 75m/s (figure 8)

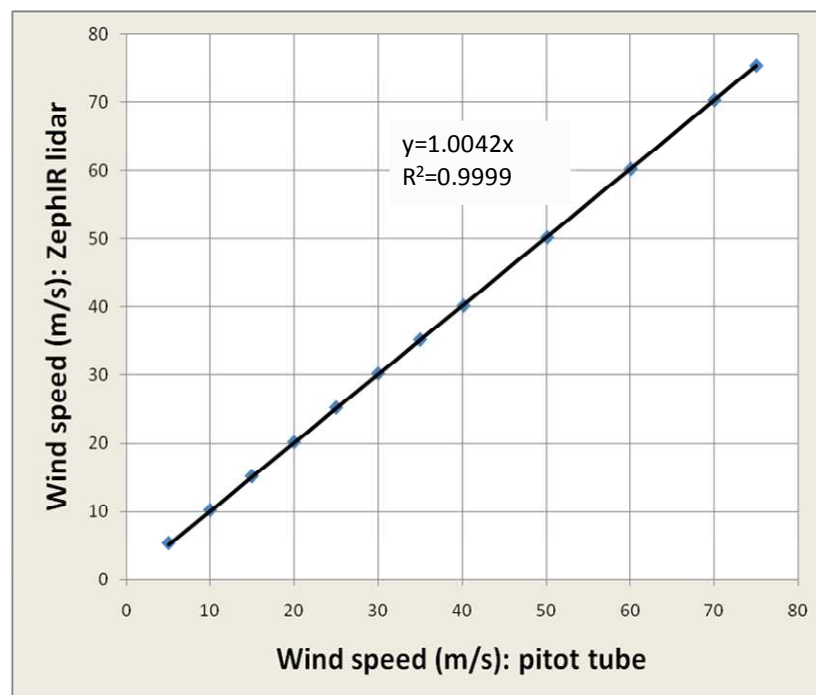


Figure 8. ZephIR lidar wind speed correlation with instrumented wind tunnel pitot tube. Courtesy of LM Wind Power, DTU Wind Energy, and NKT Photonics

A greater source of error arises from uncertainty about what provides the scattering from which the Doppler shift is derived. The scattering is assumed to originate from atmospheric particles moving at the same speed as the wind and positioned close to the focus of the lidar beam (section 3.1). An obvious example where this breaks down is when the beam intersects a solid object (e.g. a bird) that is moving at a different speed from the wind giving a measurement which could be in error. However, in such a case the value of  $\langle V_{\text{LOS}} \rangle$  so derived will stand out as clearly anomalous on the polar plot (figure 5). The presence of such points will be diluted by 50 or more correct values of  $\langle V_{\text{LOS}} \rangle$  obtained from object-free parts of the atmosphere, and their inclusion should not introduce any bias. A further safeguard against these erroneous points is provided by a simple “outlier removal” algorithm. This

identifies points that lie anomalously far from the best fit solution to eqn. (4.10) and eliminates them. The least-squares routine is then rerun on this slightly reduced set of  $\langle V_{\text{LOS}}, \phi \rangle$  data pairs.

Another example of filtering that can be required is for the case of turbine blades. For a turbine mounted lidar, situated on the roof of a turbine's nacelle, and scanning upwind through the turbine blades, the lidar must contend not only with quasi-periodic blocking of the beam, but also strong Doppler returns from the blades themselves. Although the intensity of the back reflected laser signals can be very high from these blades (typically 50 times higher than the wind returns), this can help distinguish them from the line of sight Doppler returns from the incoming wind. Additionally, the relatively slow, near perpendicular path of the blade surfaces means that the Doppler shifts are relatively low frequency (giving Doppler returns of typically  $< 2 \text{ ms}^{-1}$  or so). So efficient blade rejection filters, which remove these signals from the wind field fitting process, are simple to implement. However, blade effects do reduce the number of data points around the scan, and for all these reasons, hub (or spinner) mounted CW lidars can have some advantages.

The presence of precipitation within the probe volume leads to a different source of uncertainty. The downward motion of rain and snow inevitably leads to some error in the vertical component of wind speed. However, the presence of rain and snow is normally easily identified from the measurement process (for example by detecting activation of a rain sensor), and the resulting values can be flagged as precipitation-affected in the data. Other wind parameters are unaffected and can still be correctly inferred.

## 5.2 Cloud effects

Continuous-wave (CW) laser wind profilers focus the beam in order to measure wind speed at a given range. This technique has the advantage of uniformly high sensitivity independent of focus measurement range, and of very small probe lengths at lower ranges where detailed investigation of shear or accurate prediction of high turbulence wind fields is important. However, the signals do require correct processing when the beam impacts a cloud base at higher altitude since the contribution to the Doppler signal from cloud provides an additional contribution to that from the aerosols at the desired height.

A general approach to mitigating this problem needs first to identify the presence of a cloud return and then remove its contribution from the Doppler spectra. Cloud returns have a number of characteristics that allow them to be distinguished from aerosol returns:

- Velocity usually higher
- Spectral width usually narrower
- For horizontally scanned lidars, only part (generally the upper part) of the circular scan might be affected by cloud
- Power in Doppler peak has clear dependence on lidar focus; the power is maximised when the lidar beam is focused close to the height of the cloud base.
- Doppler spectrum is independent of focus range

The latter two characteristics are highly dependable and form the basis for identification and elimination of spurious cloud returns.

The general strategy for removal of cloud signals for a ground based, vertical scanned lidar is outlined in the following steps (and illustrated in figure 7):

1. Routinely run the lidar at an additional greater height (e.g. 800m – essentially a collimated beam output) immediately before or after the maximum height of interest, say 150m for the sake of argument.
2. For each azimuth angle around scan at 150m, identify the 800m (“cloud”) spectrum obtained at the closest value of azimuth angle.

3. Apply test conditions to the 150m spectra to determine whether any cloud signal is present in the spectral data; apply cloud removal algorithm.
4. Run standard thresholding and centroiding routines on resulting “clean” spectra and fit to the rectified cosine wave (equation (4.10)) as usual to obtain wind parameters.

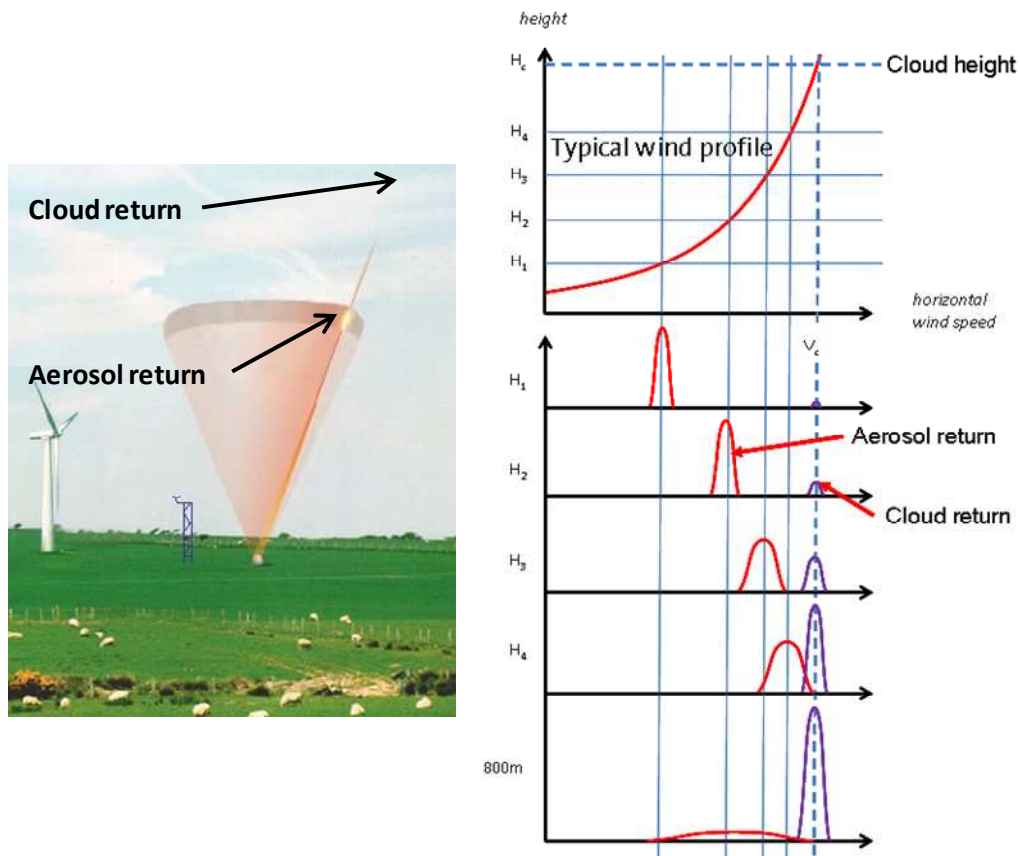


Figure 9: Cloud removal for a vertical scan CW lidar. The left plot shows the lidar conical scan focused at a typical height above ground level. The Lorentzian sensitivity curve is also shown; a spurious return is generated when the far wing of this curve intersects a strongly scattering low cloud layer. The right plot shows the aerosol (red) and cloud (purple) returns as the lidar is focused at various heights – the level of cloud contamination increases with focus height. The cloud signal is easily identified from the 800m focus, and these data are then used to eliminate the cloud return at the measurement heights.

A cloud removal algorithm based on this approach is implemented in ground based ZephIR; this has been extensively tested in a number of locations, and its effectiveness demonstrated by correlation analysis against calibrated tall masts. During the 800m (“wind profile”) scan, background measurements are taken to quantify the specific cloud return and any cloud effect is then removed from the processed data.

In general, lidars of various types of design will all have difficulty measuring in very low cloud and fog scenarios where the light emitted from the lidar is unable to reach all the ranges of interest due to absorption in the atmosphere. While this atmospheric condition mostly occurs during low wind speed periods, it is important that these periods be identified. In the majority of cases they are removed by filtering methods.

Trials of a ZephIR unit at Risø DTU’s test site at Høvsøre [Courtney and Gottschall, 2010] took place in long periods of low cloud and hence provide a demonstration of the performance in challenging cloud conditions. Cloud height was measured using a ceilometer; 25% of data was obtained with the cloud base below 300m, and 43% obtained with the cloud

base below 600m. A more recent independent evaluation of a ZephIR 300 system in similar conditions is available at: [https://www.yourwindlidar.com/sites/default/files/images/ZephIR-301-EvaluationTest\\_2011.pdf](https://www.yourwindlidar.com/sites/default/files/images/ZephIR-301-EvaluationTest_2011.pdf).

The results of this trial (Table 1) indicate a good agreement between lidar and mast at all heights from 40m up to 116m. Filtering has been applied to remove sectors prone to the influence of turbine wakes, and speeds below  $4 \text{ m s}^{-1}$ , to ensure measurement within the calibration range of the mast cups.

Height AGL (m)	Slope (m)	R <sup>2</sup>
116.5	0.993	0.977
100	0.987	0.988
80	0.984	0.992
60	0.990	0.992
40	1.007	0.992

*Table 1: Results of correlation analysis (10-minute averaged horizontal wind speed) of a ZephIR 300 trial at Høvsøre, Denmark in March 2011. A gradient  $m$  (forced through the origin) and correlation coefficient  $R^2$  both of value 1.00 would imply perfect agreement between lidar and mast-mounted cup anemometer. It should be noted that the slopes very close to 1.0 are slightly fortuitous, since the cup anemometer measurements have uncertainties at least of order  $\pm 1\%$ , due to calibration and mounting/shadowing effects.*

### 5.3 System positioning accuracy

Correct alignment ensures the risks are low, but errors in aligning the lidar during set-up will have an impact on the measurement of wind parameters. For example, for nominally vertical axis scans, wind bearing (if the lidar is rotated from its correct orientation) and vertical wind speed (if the lidar is tilted, so that the axis of its conical scan is not precisely vertical) can be affected. For a small tilt angle  $\delta$ , the error in vertical wind speed  $V_v$  will vary from  $\pm V_H \sin \delta$  (if the tilt is towards or away from the direction of the wind) to zero (if the tilt is perpendicular to the wind). Any bias on  $V_H$  is negligible to first order.

### 5.4 Probe volume effects and operation at greater ranges

As discussed in section 4.2, the lidar samples the motion of air from a finite volume, centred on the beam waist at the focus. Clearly there is minimal risk of bias while all the air within the probe volume moves at the same speed; however, for vertical scan lidars, there is usually some degree of shear across the sample region. For a linear shear this leads to spectral broadening of the returns, but no overall bias. A strong non-linear shear profile across the probe volume is required to induce any bias of significance; in practice such conditions will be rare, certainly for measurement heights around hub height and below where the probe length is relatively small.

Most lidar comparisons have taken place beside masts of heights around 100m or less. However, in early 2009 a study took place in Iowa, USA against a 200m mast in flat terrain. The results showed high correlation (Table 2, taken from [Barker, 2009]) even at the greater heights examined (150m and 200m), which approach the expected maximum operating range for focused CW lidar.

Height AGL (m)	NRG IceFree3				NRG MAX#40C			
	Ten Minute Average		Hourly Average <sup>[2]</sup>		Ten Minute Average		Hourly Average <sup>[2]</sup>	
	R <sup>2</sup>	Slope <sup>[1]</sup>	R <sup>2</sup>	Slope <sup>[1]</sup>	R <sup>2</sup>	Slope <sup>[1]</sup>	R <sup>2</sup>	Slope <sup>[1]</sup>
193	0.984	0.987	0.987	0.987	0.982	0.993	0.988	0.992
157	0.982	1.006	0.988	1.005	0.984	1.001	0.989	1.000

Table 2: Results of a comparative trial of a ground-based, vertical scan ZephIR lidar against a very tall mast, equipped with two types of cups at each height. The data indicate that the extended probe length at greater heights did not result in excessive bias or errors. [1]: Forced through the origin; [2]: Only hourly averages containing 6 valid 10-minute measurements compared.

### 5.5 Flow uniformity and complex terrain

Because only line-of-sight wind components are measured, a single ground-based lidar unit inevitably provides an incomplete picture of the 3D vector flow, regardless of the scan pattern employed. Firstly, this “cyclops” LOS velocity determination at any one probe point is unable to disambiguate the full wind vector information, merely measuring one component. The full vector at a given point can only be measured by the provision of three (or more) lidar units positioned on the ground at an appropriate separation distance (comparable to the measurement height for best accuracy), such as the Windscanner system under development by Risø DTU, web address below:

[http://www.risoe.dtu.dk/research/sustainable\\_energy/wind\\_energy/projects/vea\\_wind\\_scanner.aspx?sc\\_lang=en/](http://www.risoe.dtu.dk/research/sustainable_energy/wind_energy/projects/vea_wind_scanner.aspx?sc_lang=en/)

Secondly, whilst a given scan pattern can provide more information about the wind flow, certain assumptions e.g. uniformity of flow across the probed area, linear or logarithmic vertical shears, are often reasonably made. However, in complex terrain, the flow undergoes stable and unstable non-uniformities, and the figure-of-eight plot (figure 6) can distort systematically for a given wind direction, reflecting the speeding up and slowing down in certain regions of the scan. The ZephIR lidar provides some information about the flow non-uniformity, with up to 50 points per second being interrogated around the scan disk.

In the presence of non-uniformity in flow (section 3.2), a lidar measurement can indicate a wind speed different to that from a point measurement by a mast-mounted cup anemometer. Work is ongoing to combine lidar data with the output from flow-modelling software, using both linear models [Bingøl et al, 2008; Bingøl et al, 2009; Bingøl, 2009] and computational fluid dynamics, CFD [Harris et al, 2010; Pitter et al, 2012]. This pragmatic approach generates measurements equivalent to a “point-in-space” sensor by using the results of flow modelling to adjust the lidar wind speed. This topic will be dealt with elsewhere in this lecture series, examining possible improvement of lidar resource assessment capability in complex terrain.

### 5.6 Dependence on backscatter level

Under conditions of high backscatter, the spectrum provides an accurate measure of the distribution of line-of-sight velocities within the probe volume, weighted according to eqn. 4.1. As the backscattering strength drops (usually associated with increased air clarity) this has a similar effect to raising the detection threshold (section 4.8), and will lead to elimination from the spectrum of weaker components of velocity. The impact of the system noise floor on the detailed spectral shape will also be increased. The centroid values  $\langle V_{LOS} \rangle$  will be unbiased and independent of threshold level when the spectrum is symmetrical. However, for a skewed (asymmetric) spectrum the precise value of  $\langle V_{LOS} \rangle$  can be sensitive to the threshold. Hence a small difference in measured wind speed is possible between two

measurements under conditions that are identical in every way apart from the level of backscatter. However, there is no evidence from comparisons so far to suggest that this leads in practice to a significant discrepancy.

A further possibility to be considered is the effect of saturation (by very strong scattering returns from thick cloud) of the lidar detector, electronics or signal processing. In the event that the input signal exceeds these limits, the spectrum will become distorted, possibly featuring higher harmonic components of the true Doppler frequencies. In practice, the range of inputs to the ADC can be tailored to accommodate the highest levels of backscatter that will reasonably be encountered, eliminating the risk of bias.

### **5.7 Beam obscuration and attenuation**

Lidar can operate successfully even when part of its scan is obscured. This confers great flexibility so that the system can easily be located adjacent to masts, buildings, in forests or the aforementioned horizontal scan through moving turbine blades. Stationary objects pose no major problem other than the loss of wind measurements from the relevant obscured sector of the scan. Slowly moving objects can also easily be filtered, based on the magnitude of their Doppler shift.

In the above cases, the fit to eqn. (4.10) will no longer contain data over the full 360 degree range of  $\phi$ . Laboratory experiments on moving belt targets have indicated that accurate measurements are obtained even when over half of the scan is obscured. Catastrophic errors in the least-squares fitting process become possible as the obscuration increases yet further; such conditions are identified and a null result returned.

### **5.8 Wind direction**

For ground based, vertically scanning ZephIR, the two best-fit solutions obtained to eqn. (4.10) by give values of wind direction that are 180 degrees apart. Selection between the two options is made with reference to the measurement of wind direction from a ground-based anemometer. This needs to be in disagreement by over 90 degrees with the direction at the chosen height for the incorrect choice to be made. While such a directional shear (veer) is conceivable in highly complex terrain and at very low wind speed, it is much less likely in the reasonably uniform conditions of interest for wind energy applications. In the event of the wrong choice being made, leading to a wind direction that is in error by 180 degrees, the value of vertical component of the wind  $V_v$  will have the wrong sign. In other words, an updraught will be wrongly identified as a down draught (of the same absolute speed) and vice versa.

## 6. Calibration, validation and traceability

For historical reasons, the clearest demonstration of validity is provided by direct side-by-side comparisons between the lidar system and a fully instrumented IEC-compliant meteorological mast of suitable height. Rigorous comparisons must be carried out with great care to avoid a number of problems associated with cup anemometers [Kristensen, 1999]. These are well known and include the following:

- Shadowing of the cup anemometer by the mast from certain directions.
- Cup overspeeding in turbulence and sensitivity to any vertical wind component
- Cup icing
- Valid cup anemometer calibration.
- Topographic effects leading to non-uniform flow across the area occupied by mast and lidar scan (including turbine wakes).

A lidar/mast comparison is commonly used to provide a validation of lidar performance, and examples of such checks were provided by the results in Tables 1 and 2. The lidar can then be used as a traceable reference for comparison with other units.

Lidar systems are normally calibrated in the laboratory before shipping. Routine checks on the calibration of units on their return to base provide confidence of long-term stability. As an example, the calibration process undertaken for a ZephIR lidar is outlined below. This consists of three stages:

- Velocity and direction check against a calibrated moving belt. The process provides a direct check of laser wavelength and scanner cone angle, each of which affects the velocity calibration (via eqn. (4.4) and (4.11) respectively).
- A focus range check is carried out with a moving target located at precise distances from the lidar. The closed loop positioning system using a linear encoder ensures no drifts over time. An example of the output data from a focus calibration test was plotted in figure 4 (section 4).
- Finally, each unit undergoes an outdoor test to measure wind speed at several heights using an industry-certified, 92m, meteorological mast. Figure 8 shows an example correlation plot of 10-minute average horizontal wind speed, obtained over a period of 7 days.

Each of the three tests above gives information on the sensitivity of the unit; for deployments in “clean” air, it is important to ensure this aspect of performance is fully optimised and has not deteriorated, or there is a risk of reduced data availability.

It is important that no adjustments are performed during validation trials, or afterwards for as long as the lidar remains a traceable reference unit. The certification process outlined above has been defined in collaboration with industry experts including Garrad Hassan and provides the traceability that is a key element of formal energy prediction reports used by the financial community.

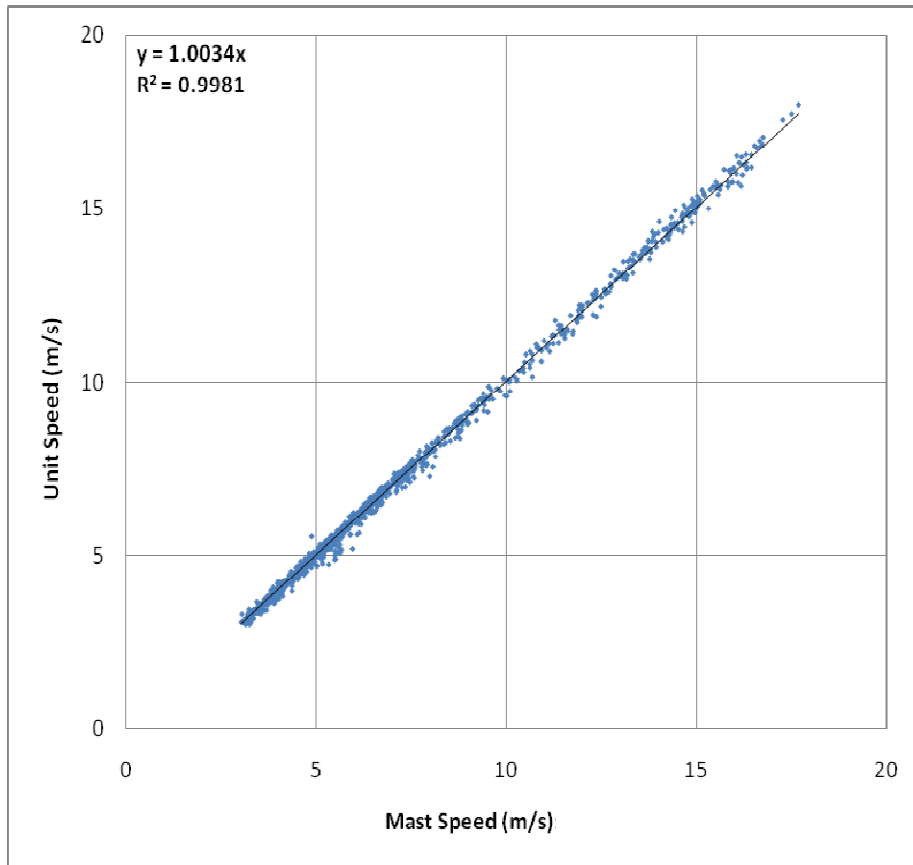


Figure 10: A ground based ZephIR 300 system is compared to the Pershore, industry-certified metmast, showing strong correlation and a gradient close to unity. In this example, comparison was carried out at 70.5m altitude. From [Rutherford et al, 2012].

In addition to its velocity measurements being closely traceable to primary units of time and length, lidar offers a potential advantage for accurate shear profiling (both for speed and direction) in that the same instrument is used to make the measurements at all heights. By contrast, a mast relies on consistent calibration of the full set of cups and vanes; any differences in calibration of the individual instruments will lead to uncertainty and error in the shear assessment. An example of the difficulty in calibrating instruments (such as cup anemometers) that rely on relatively complex, non-linear physical interactions is illustrated in figure 11, where calibration results from a pair of high quality cup anemometers are compared.

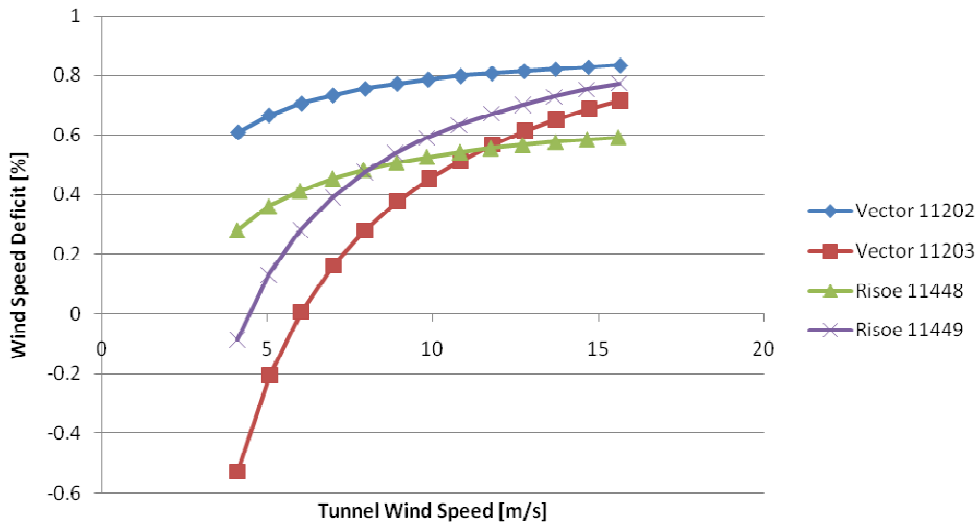


Figure 11. Graph showing results from routine re-calibration of 4 cups to be used at an accredited met mast site . The vertical axis shows differences when the same cup was calibrated at two independent wind tunnel standards facilities. The tunnel-to-tunnel calibrations of the same cups show variability of the order of 1%.

In contrast to the significant performance variations in cup anemometers that are considered to be a wind industry primary benchmarks, even in the somewhat idealised and highly controlled conditions inside a windtunnel, lidars can show repeatable performance. In a recently published study [Rutherford] agreement in mean wind speed with a 92 m tall mast to better than 99% is obtained across a batch of 28 production ZephIR lidars at all heights tested (table 3)

Combined results from 28 ZephIR300 units						
Height (m)	Gradient		R <sup>2</sup>		Laser Sensitivity	
	Mean	Std Dev	Mean	Std Dev	Mean	Std Dev
91	1.0039	0.0072	0.9894	0.0059	1.0350*	0.0893
70	1.0033	0.0072	0.9928	0.0038		
45	1.0005	0.0050	0.9924	0.0050		
20	0.9967	0.0045	0.9925	0.0048		

Table 3. The mean and standard deviation of the mast correlation parameters, gradient and R<sup>2</sup>, have been calculated from the first batch of 28 ZephIR300 units. These results confirm the consistency of the lidars' performance.

## 7. Summary, state of the art, and future developments

Coherent monostatic CW lidar is a method capable of rapid wind speed measurement at relatively short ranges (all the way from 10m to 200m) and hence is well suited to several requirements in the field of wind energy. Examination of the measurement process reveals that the basic acquisition of line-of-sight Doppler spectra is a well-established method with little scope for gross errors and miscalibration. The subsequent steps required to convert these spectra into a profile of wind speed are more complex, however, and their validity relies on a number of well-established assumptions. Much work has been performed to test the validity of assumptions outlined in section 3, and to understand the uncertainties and other issues discussed in section 5.

Complex terrain remains a topic of great interest as it becomes increasingly necessary to explore less ideal locations as potential wind farm sites. In such sites the horizontal wind speed deduced by conically-scanned lidar can be subject to differences in comparison to that measured by co-located cup anemometers when the flow is non-uniform across the lidar measurement disk. A method has recently been developed in which the impact of inhomogeneous flow at complex flow sites is examined using Computational Fluid Dynamics (CFD) modelling to predict the bias that will be experienced by a lidar in comparison to a conventional met mast equipped with cup anemometers. Similar percentage changes in wind speed as measured by a mast are shown to occur if the mast were to be moved by  $\pm 50\text{m}$  from its original location. This suggests a methodology for resource assessment in complex terrain in which lidar is used in combination with CFD modelling in order to (i) adjust the lidar data for the impact of non-uniform flow and (ii) investigate the wind variations across the site that are a major source of uncertainty for current techniques.

Lidar offers some potential advantages in turbine power curve measurement. The measurement over an extended volume may give a more representative estimate of the wind energy content of the air interacting with the blades, and the ability to re-position the lidar quickly is clearly advantageous. A study reported by [Wagner et al 2008] has shown that exploiting the lidar wind profile data can reduce the scatter of points in a measured power curve. In another recent study [Cayla, 2010] a ZephIR lidar gave an almost identical power curve to an IEC-instrumented power performance mast. The scatter of the points in the power curve obtained using the ZephIR data at hub height was somewhat lower than that for the mast. This result needs further investigation and possibly is a consequence of the more effective sampling of the wind around the scan disk. It follows, interestingly, that remote sensing equipment that agrees perfectly with the mast would therefore have provided higher scatter in the power curve than ZephIR!

The extraction of turbulence data relevant to the wind industry from lidar signals is an area that will benefit from further research and verification through field comparisons. Turbulence can manifest itself as gusts, eddies, and fluctuations in wind speed. It is important in wind energy applications to characterise the levels of turbulence encountered at a specific site location. A commonly-used basic measure of turbulence is turbulence intensity (TI). ZephIR calculates the turbulence intensity that a conventional cup would have obtained at the same measurement height by analysing the variation in individual wind speed values during a 10-minute averaging period. This value of TI is automatically logged in the output data. The calculation takes into account the difference between point measurements obtained from a cup anemometer, and spatially-averaged lidar data where a volume is interrogated [Barker et al, 2012]. ZephIR's measurements of turbulence have been investigated in a number of independent studies against calibrated met masts in flat, offshore and complex terrain, and at different heights above ground [Wagner et al, 2009].

Resource assessment in maritime locations is becoming increasingly relevant as offshore wind farms assume greater importance. The cost of installing an offshore tall mast is very high, so remote sensing may prove particularly advantageous in such locations. ZephIR lidars have been involved in successful trials on several offshore platforms [e.g. Pena et al, 2008] in the North Sea, the Baltic, and around the lakes and coasts of North America. A floating lidar platform offers an exciting future concept; an early attempt to develop a ZephIR system on a buoy (SeaZephIR) took place in 2004/5. After a redesign, the system took to the water off S Norway in 2009. A world-first demonstration trial took place over a period of several weeks in late 2009, involving one ZephIR unit stationed on land, with the floating SeaZephIR unit positioned 800m out to sea. The wind speeds measured by the two ZephIR units showed excellent correlation, with differences in mean wind of  $\sim 1\%$  or less at all heights over a 3 week test period (see Table 4, from [Wiggins, 2009]). In this trial there was no attempt to compensate for the platform motion; it may be necessary in very severe conditions to use measurements of the 6 degrees of freedom (3 rotational and 3 translational) that can in

principle distort the lidar measurement. The low impact of the motion observed in trials so far may be a consequence of the high stability of the buoy combined with the very fast 50Hz measurement rate for the ZephIR lidar, which allows a snapshot of the wind around a 360-degree disk to be obtained in 1 second. Further development of SeaZephIR is ongoing.

Height AGL (m)	Slope (m)	R <sup>2</sup>
120	0.993	0.972
90	0.998	0.970
60	1.004	0.968
30	0.990	0.954
10	0.984	0.953

*Table 4: Correlation analysis from the first SeaZephIR trial (2009): the table shows gradient (m) and correlation coefficient (R<sup>2</sup>) for plots of 10-minute wind speed for SeaZephIR on a floating platform versus those measured by a second ZephIR unit positioned 800m away on land.*

Forward-looking turbine mounted lidar, either on the nacelle or in the hub, is another exciting lidar development. Applications include turbine power curve measurement, energy yield optimisation (e.g. by reducing turbine yaw misalignment) and gust and fatigue load reduction allowing longer turbine lives and/or turbine build cost reduction. As already remarked, CW lidar seems particularly well suited to this type of application, owing to its high sensitivity (high average photon flux), high sample rate (50 Hz), and scan path that probes the wind around the rotation path of the rotor. Another of its benefits is its flexibility in terms of turbine mounting. In addition to nacelle roof mounting, it is, to date, the only class of lidar that has been installed in a rotor hub (or spinner).

Interest in these concepts has increased significantly since the world-first proof-of-principle demonstration of turbine-mounted lidar in 2003 [Harris et al, 2006 and 2007], with several groups currently working towards evaluating the concept. Developments include incorporation of a conical-scanning ZephIR lidar in the spinner of a large turbine [Mikkelsen et al, 2010; Angelou et al, 2010] giving an unobscured view of the approaching wind. More recent still has been R&D activity funded by the Danish High Technology Fund [DHTF] studying implementation of CW turbine blade mounted lidar. Here the concept is to have a ZephIR base unit installed in a turbine hub, connected by fibre optics to small, fixed focus telescopes mounted on the blades of the turbine. The rotation of the blades naturally allows scanning of the wind field around the blade path, and this approach holds some promise for blade pitch optimisation, for example. Initial experiments in a wind tunnel (figure 12) [Pedersen et al 2012] have confirmed the potential of the approach and turbine trials are due to commence shortly.

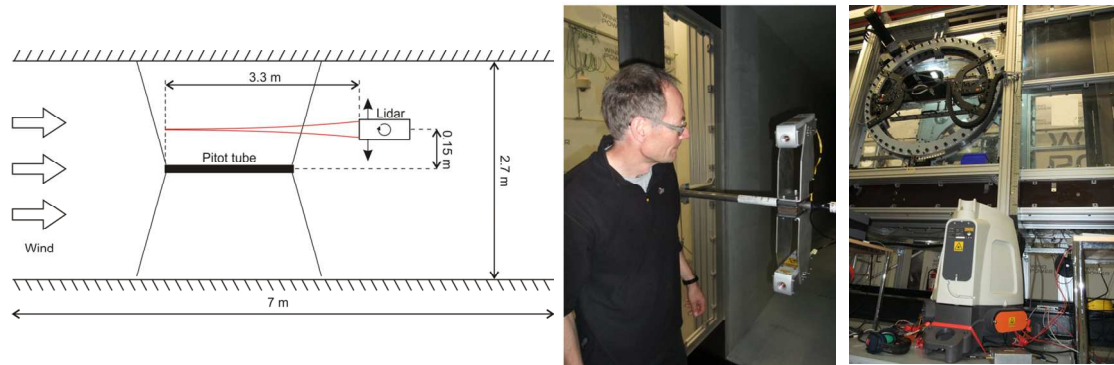


Figure 12. CW lidar experiments in a wind tunnel, prior to blade lidar deployment experiments. L: wind tunnel schematic. M: CW lidar twin telescopes. R: External view of the wind tunnel, showing the ZephIR 300 base unit.

In connection with turbine mounted lidars, significant recent efforts in the industry have focussed on quantifying their potential benefits, as well as looking at the optimum lidar configurations to use. For CW lidars, the cone scan angle, the number of ranges to scan over (if indeed more than one is required), scan rates and the LOS processing algorithms are all being investigated. Recent results in the literature have included:

1. Conical scan CW lidar was used to determine yaw alignment of a lidar in a study by Kragh et al [Kragh et al, 2012], and demonstrated the ability to achieve a sub  $4^\circ$  yaw error over a 2 hour period, even during periods of high turbulence.
2. Simulations examining the ability of turbine mounted lidar for accurate yaw alignment by Kragh et al [Kragh et al, 2011] indicated yield, at below rated power, could be raised by 1% to 5%.
3. A study reported in [Schlipf et al, 2011], comparing conventional nacelle based wind vane with lidar yaw alignment control, indicated that the yearly energy output of a 5 MW turbine could be enhanced by  $\sim 2\%$  using the lidar.
4. Schlipf and Kuhn [Schlipf and Kuhn, 2008] modelled the benefits of a nacelle mounted lidar for feedforward control, in particular turbine speed control. The study found reductions in standard deviations of 91%, 90% and 71% for rotor speed, tower fore-aft moment and blade root flap moment for gusts. For turbulent airflows, the reductions in standard deviations were 77%, 32% and 17% respectively.
5. Simley et al [Simley et al, 2011] simulated a conical scan CW lidar and showed accurate yaw alignment should be possible. Even in highly turbulent airflow, a precision of a few degrees was achievable. The same paper also showed that RMS wind speed measurement errors were lower for a CW system than a pulsed system for ranges  $<125\text{m}$
6. Simulations using lidar feedforward control by Laks et al [Laks et al, 2011] showed turbine fatigue load reductions of approximately 20%.
7. A very recent study by Rogers et al of DNV [Rogers et al, 2012] analysed a variety of scenarios that could be addressed by turbine mounted lidar, including retrofitting lidar to existing turbines, larger rotors and taller towers. Benefits of turbine mounted lidar included a 6 year life extension and 30% total yield in energy production (when a lidar was retrofitted to a 2.5 MW turbine); an increase in permitted rotor area of 6% and an associated energy output increase of 4% (larger rotor on 5 MW turbine); a 3% energy output increase from a increased allowable tower height, achieved through reduced fatigue loads (again on a 5

MW turbine). The same study also estimated an achievable increase in energy output due to optimisation of lidar control alone to be just 0.6%.

Clearly, turbine mounted lidars have an important role to play in reducing costs of energy generated by wind turbines. This application is discussed in more detail and in broader scope in other lectures.

**Acknowledgements:** The authors are grateful for the support and enthusiasm of their colleagues and collaborators. Without them, wind power lidar technology could not have evolved to its current advanced state.

## 8. References

- N Angelou, T Mikkelsen, K H Hansen, M Sjöholm, M Harris, "LIDAR Wind Speed Measurements from a Rotating Spinner: SpinnerEx 2009", Project Upwind and Risø report Risø-R-1741(EN), August (2010).
- V A Banakh, I N Smalikho, F Köpp & C Werner, "Representativeness of wind measurements with a CW Doppler lidar in the atmospheric boundary layer", *Applied Optics* **34** 2055-2067 (1993)
- V A Banakh, I N Smalikho, F Köpp & C Werner, "Measurements of turbulent energy dissipation rate with a CW Doppler lidar in the atmospheric boundary layer", *J. Atm Oceanic Tech.* **16** 1044-1061 (1999)
- W Barker, "Analysis of ZephIR data from Mason City, Iowa", internal report, Natural Power (2009)
- W Barker, M Pitter, E Burin de Roziers, M Harris, R Scullion, "Can lidars measure turbulence", EWEA conference PO74, Copenhagen (2012).
- F Bingöl, J Mann & D Foussekis, "Lidar error estimation with WAsP engineering", *IOP Conf. Series: Earth and Environmental Science* **1** 012058 (2008)
- F Bingöl, J Mann & D Foussekis, "Conically scanning lidar error in complex terrain", *Met. Zeitschrift* **18** 189-195 (2009)
- F Bingöl, "Complex terrain and wind lidars", Risø-PhD-52(EN) (2009)
- B I Bleaney & B Bleaney, "Electricity and Magnetism", Oxford University Press, Section 23.4, (1976)
- M Cayla, "Comparison of ZephIR measurements against cup anemometry and power curve measurements", internal report, Natural Power (2010)
- M L Chanin, A Gariner, A Hauchecorne & J Portneuve, "A Doppler lidar for measuring winds in the middle atmosphere", *Geophys. Res. Lett.* **16** 1273-1276 (1989)
- S F Clifford & S Wandzura, "Monostatic heterodyne lidar performance: the effect of the turbulent atmosphere", *Applied Optics* **20** 514-516 (1981)
- M Courtney & J Gottschall, "ZephIR 145 validation test", Risø DTU report for Natural Power (2010)
- DHTF. "HTF number 049-2009-3 - Integration of wind LIDAR's in wind turbines for improved productivity and control", a Danish National Advanced Technology Foundation's (DNATF) Project.
- R M Hardesty & B F Weber, "Lidar measurement of turbulence encountered by horizontal-axis wind turbines", *J Atmos. and Oceanic Tech.*, **4** 191-203 (1987)
- M Harris, G N Pearson, C A Hill & J M Vaughan, "Higher moments of scattered light fields by heterodyne analysis", *Applied Optics* **33** 7226-7230 (1994)
- M Harris, G Constant and C Ward, "Continuous-wave bistatic laser Doppler wind sensor", *Applied Optics* **40** 1501-1506 (2001a)
- M Harris, G N Pearson, K D Ridley, C J Karlsson, F Å A Olsson & D Letalick, "Single-particle laser Doppler anemometry at 1.55 $\mu\text{m}$ ", *Applied Optics* **40** 969-973 (2001b)
- M Harris, M Hand & A Wright, "Lidar for turbine control", Technical Report NREL/TP-500-39154 (2006)
- M Harris, D J Bryce, A S Coffey, D A Smith, J Birkemeyer, U Knopf, "Advance measurements of gusts by laser anemometry", *J. Wind Engineering and Industrial Aerodynamics* **95** 1637-1647 (2007)

M Harris, I Locker, N Douglas, R Girault, C Abiven & O Brady, “Validated adjustment of remote sensing bias in complex terrain using CFD”, EWEC Proceedings (2010)

A V Jelalian, “Laser radar systems”, Boston: Artech (1992)

C J Karlsson, F Å A Olsson, D Letalick & M Harris, “All-fiber multifunction CW 1.55 micron coherent laser radar for range, speed, vibration and wind measurements”, Applied Optics **39** 3716-3726 (2000)

D Kindler, A Oldroyd, A MacAskill & D Finch, “An 8 month test campaign of the QinetiQ ZephIR system: preliminary results”, Extended Abstracts of the Intern. Symp. for the Advancement of Boundary Layer Remote Sensing (ISARS 13), 18-20 July 2006, Garmisch-Partenkirchen, Germany. Wiss. Ber. FZKA 7222, 165-167

L Kristensen, “The perennial cup anemometer”, Wind Energy **2** 59-75 (1999)

K A Kragh and M H Hansen “Individual Pitch Control Based on Local and Upstream Inflow Measurements.” In: Proceedings of 49th AIAA Aerospace Sciences Meeting including the New Horizons Forum and Aerospace Exposition; American Institute of Aeronautics and Astronautics, AIAA 2011-813, 4 - 7 January 2011, Orlando, Florida (2011).

K A Kragh, M H Hansen and T Mikkelsen, “Precision and shortcomings of yaw error estimation using spinner-based light detection and ranging”. Accepted for publication in: Wind Energy, (2012).

L Lading, S Hanson & A Skov Jensen, “Diffraction-limited lidars: the impact of refractive turbulence”, Applied Optics **23** 2492-2497 (1984).

J Laks, L Y Pao, E Simley, A Wright, N Kelley, B Jonkman. “Model Predictive Control Using Preview Measurements From LIDAR”. In: Proceedings of 49th AIAA Aerospace Sciences Meeting including the New Horizons Forum and Aerospace Exposition; American Institute of Aeronautics and Astronautics, AIAA 2011-813, 4 - 7 January 2011, Orlando, Florida (2011).

R Loudon, “The quantum theory of light”, 3<sup>rd</sup> edition, Oxford University Press (2000)

T Mikkelsen, K Hansen, N Angelou, M Sjöholm, M Harris, P Hadley, R Scullion, G Ellis & G Vives, “Lidar wind speed measurements from a rotating spinner”, EWEC Proceedings (2010).

G N Pearson, P J Roberts, J R Eacock & M Harris, “Analysis of the performance of a coherent pulsed fiber lidar for aerosol backscatter applications”, Applied Optics **41** 6442-6450 (2002)

A T Pedersen, B F Montes, J E Pedersen, M Harris, and T Mikkelsen, “Demonstration of short-range wind lidar in a high-performance wind tunnel”, EWEA conference PO78, Copenhagen (2012).

A Peña, CB Hasager, SE Gryning, M Courtney, I Antoniou, T Mikkelsen “Offshore wind profiling using light detection and ranging measurements”. Wind Energy 12:105–124 (2009)

M Pitter, C Abiven, M Harris, W Barker, O Brandy, “Lidar and computational fluid dynamics for resource assessment in complex terrain”, EWEA conference PO80, Copenhagen (2012).

T Rogers, A Byme, T McCoy, K Briggs, “Expected impacts on cost of energy through lidar based wind turbine control”, EWEA 2012, Apr 17, (2012)

A Rutherford, M Harris, W Barker, E Burin de Roziers, R Pitter, R Scullion, C Slinger, “Lidar calibration and performance validation process” AWEA conference, Atlanta, (2012).

D Schlipf and M Kuhn, “Prospects of a collective pitch control by means of predictive disturbance compensation assisted by wind speed measurements”. In: German Wind Energy Conference (DEWEK), (Bremen, Germany), pp. 1–4, (2008).

D Schlipf, J Anger, S Kapp, O Bischoff, M Hofsäß, A Rettenmeier, M Kühn, "Prospects of optimization of energy production by lidar assisted control of wind turbines". In: Proceedings of European Wind Energy Conference and Exhibition, EWEA 2011, Brussels (B), 14-17 March, (2011).

E Simley, L Y Pao, R Frehlich, B Jonkman, N Kelley "Analysis of Wind Speed Measurements using Continuous Wave LIDAR for Wind Turbine Control". In: Proceedings of 49th AIAA Aerospace Sciences Meeting including the New Horizons Forum and Aerospace Exposition. American Institute of Aeronautics and Astronautics, AIAA 2011-263, 4 - 7 January 2011, Orlando, Florida (2011).

D A Smith, M Harris, A S Coffey, T Mikkelsen, H E Jørgensen & J Mann, "Wind lidar evaluation at the Danish wind test site in Høvsøre", *Wind Energy* **9** 87-93 (2006)

C M Sonnenschein & F A Horrigan, "Signal-to-noise relationships for coaxial systems that heterodyne backscatter from the atmosphere", *Appl. Opt.* **10** 1600-1604 (1971)

A E Siegman, "Lasers", Mill Valley, California: University Science Books (1986)

J M Vaughan & P A Forrester, "Laser Doppler velocimetry applied to the measurement of local and global wind", *Wind Engineering*, **13** 1-15 (1989)

R Wagner, T Mikkelsen & M Courtney, "Investigation of turbulence measurements with a continuous-wave conically scanning lidar", *Risø-R-1682(EN)* (2009)

R Wagner, H E Jørgensen, U S Paulsen, T J Larsen, I Antoniou, L Thesbjerg, "Remote sensing used for power curves", *IOP Conf. Series: Earth and Environmental Science* **1** 012059 (2008)

J Wiggins, unpublished internal report, Natural Power (2009)

J A Zak "Atmospheric boundary layer sensors for application in a wake vortex advisory system", *NASA/CR-2003-212175*